Article:
Paddock, R. W., Li, T. S., Kim, E. et al. (25 more authors) (2024) Energy gain of wetted-foam implosions with auxiliary heating for inertial fusion studies. Plasma Physics and Controlled Fusion. 025005. ISSN: 1361-6587

https://doi.org/10.1088/1361-6587/ad15ee

Energy gain of wetted-foam implosions with auxiliary heating for inertial fusion studies

OPEN ACCESS
IOP Publishing
Plasma Physics and Controlled Fusion
Plasma Phys. Control. Fusion **66** (2024) 025005 (10pp)
https://doi.org/10.1088/1361-6587/ad15ee

Energy gain of wetted-foam implosions with auxiliary heating for inertial fusion studies

R W Paddock[1,16,*], T S Li[2], E Kim[3], J J Lee[1,4], H Martin[1], R T Ruskov[1], S Hughes[5], S J Rose[1,6], C D Murphy[7], R H H Scott[8], R Bingham[8], W Garbett[9], V V Elisseev[1,4,10], B M Haines[11], A B Zylstra[12], E M Campbell[13], C A Thomas[13], T Goffrey[14], T D Arber[14], R Aboushelbaya[1], M W Von der Leyen[1,15], R H W Wang[1], A A James[1], I Ouatu[1], R Timmis[1,15], S Howard[1], E Atonga[1] and P A Norreys[1,2,15,*]

[1] Department of Physics, Atomic and Laser Physics Sub-Department, Clarendon Laboratory, University of Oxford, Parks Road, Oxford OX1 3PU, United Kingdom
[2] University College, University of Oxford, High Street, Oxford OX1 4BH, United Kingdom
[3] St Peter's College, University of Oxford, New Inn Hall Street, Oxford OX1 2DL, United Kingdom
[4] IBM Research Europe, The Hartree Centre, Daresbury Laboratory, Keckwick Lane, Warrington WA4 4AD, United Kingdom
[5] Trinity College, University of Oxford, Broad Street, Oxford OX1 3BH, United Kingdom
[6] Centre for Inertial Fusion Studies, The Blackett Laboratory, Imperial College, London SW7 2AZ, United Kingdom
[7] York Plasma Institute, Department of Physics, University of York, Heslington YO10 5DD, United Kingdom
[8] Central Laser Facility, STFC, Rutherford Appleton Laboratory, Harwell Campus, Didcot, Oxfordshire OX11 0QX, United Kingdom
[9] AWE plc, Aldermaston, Reading, Berkshire, RG7 4PR, United Kingdom
[10] Wrexham Glyndr Universityŵ, Mold Rd, Wrexham LL11 2AW, United Kingdom
[11] Los Alamos National Laboratory, MS T087, Los Alamos, NM 87545, United States of America
[12] Lawrence Livermore National Laboratory, Livermore, CA 94550, United States of America
[13] Laboratory for Laser Energetics, University of Rochester, Rochester, NY 14623, United States of America
[14] Centre for Fusion, Space, and Astrophysics, Department of Physics, University of Warwick, Coventry CV4 7AL, United Kingdom
[15] John Adams Institute for Accelerator Science, Denys Wilkinson Building, Oxford OX1 3RH, United Kingdom

E-mail: robert.paddock@eng.ox.ac.uk and peter.norreys@physics.ox.ac.uk

Received 28 September 2023, revised 17 November 2023
Accepted for publication 14 December 2023
Published 27 December 2023

Abstract

Low convergence ratio implosions (where wetted-foam layers are used to limit capsule convergence, achieving improved robustness to instability growth) and auxiliary heating (where electron beams are used to provide collisionless heating of a hotspot) are two promising

[16] Current address: Department of Engineering Science, University of Oxford, Oxford OX1 3PJ, United Kingdom
[*] Authors to whom any correspondence should be addressed.

techniques that are being explored for inertial fusion energy applications. In this paper, a new analytic study is presented to understand and predict the performance of these implosions. Firstly, conventional gain models are adapted to produce gain curves for fixed convergence ratios, which are shown to well-describe previously simulated results. Secondly, auxiliary heating is demonstrated to be well understood and interpreted through the burn-up fraction of the deuterium-tritium fuel, with the gradient of burn-up with respect to burn-averaged temperature shown to provide good qualitative predictions of the effectiveness of this technique for a given implosion. Simulations of auxiliary heating for a range of implosions are presented in support of this and demonstrate that this heating can have significant benefit for high gain implosions, being most effective when the burn-averaged temperature is between 5 and 20 keV.

Keywords: inertial fusion, auxiliary heating, low convergence ratio

1. Introduction

The recent progress at the National Ignition Facility (NIF) has sparked fresh excitement around the topic of inertial fusion energy (IFE) [1–5]. However, significant advances are still required before the goal of practical fusion energy can be realized. In particular, while the recently achieved gain of 1.5 represents an unprecedented milestone [5], it is still short of the minimum value of 50 likely to be required for a viable fusion reactor [6]. In addition, current target designs are expensive and time-consuming to produce [7], while cost estimates for future fusion reactors require low cost and high repetition rates [8, 9]. A comprehensive summary of the current state of IFE research is available in the Department of Energy's Office of Fusion Energy Sciences Basic Research Needs workshop report [10].

Wetted-foam capsules are seen as a promising target solution for future IFE reactors, with the potential to enable high gain performance at low cost. The CH foams used to contain the deuterium-tritium (DT) liquid fuel can potentially be 3D printed [11], which could significantly improve the production rate and cost of such targets compared to conventional DT-ice targets. A variety of designs based on this technology have been proposed and demonstrated, ranging from more conventional designs (where the wetted-foam layer replaces a DT ice layer [12]) to novel dynamic-shell approaches [7, 13].

One of the potential advantages of wetted-foam implosions is that the higher vapor densities that result from the use of liquid (rather than frozen) DT enable low convergence ratio implosions [12]. While this does limit the fusion performance, it also makes the implosion more robust to hydrodynamic instability growth and thus can lead to greater agreement between simulation and experiment. The potential performance of low convergence ratio implosions of wetted-foam capsules has been considered previously [11, 12, 14, 15], as well as in [16] where a number of implosions of different capsule radii and laser drive energy were optimized to explore the performance over a wide parameter space.

Another interesting innovation is auxiliary heating, which may be used to improve the fusion performance of such implosions. This technique (first proposed in [17], and further explored by [18, 19]) uses a relativistic electron beam to provide collisionless heating of the hotspot of an implosion (while early work on this technique stated that overlapping electron beams would be required [18], subsequent work found that using a single beam would be equally effective [19]). The electron beam leads to a 'bump-on-tail' of the electron distribution function, resulting in the growth of Langmuir waves in the hotspot. As these waves grow, electrons from the beam become trapped, and this causes the instability to saturate [20, 21]. Daughter Langmuir waves are then generated through the Langmuir wave modulation instability [22–25], and these daughter waves are effectively damped. The energy in the wave is thus transferred to electrons in the background plasma, driving an increase in the electron temperature. Collisions between electrons and ions means that this also leads to an increase in the ion temperature; this process takes place over a few picoseconds, which is fast compared to the compression timescale of the capsule.

This is inherently a multi-scale problem and is therefore difficult to simulate; radiation hydrodynamics codes are unable to simulate the Langmuir waves and Landau damping that drive the heating mechanism, but are the only codes capable of simulating a full IFE implosion. Researchers in [26] attempted to address this by simulating the effect of the heating mechanism (explored previously in a Vlasov code in [18]) by adding electron energy to the central zones of a hydrodynamic simulation at times near the bang time. These simulations focused on subignition implosions, and suggested that this technique could potentially be an effective way at improving the fusion performance of these implosions. While [16] considered direct-drive implosions, similar results have previously been demonstrated for indirect-drive implosions [27]. An ongoing collaboration between IBM Research and the University of Oxford aims to develop a multi-scale modeling capability to improve simulations of this technique, through the use of multiple different codes [28]. A radiation-hydrodynamics code is first used to simulate the implosion until the heating is applied, at which point a PIC code is used to simulate the injection of an electron beam into the plasma profile present at that time. Once the heating process has occurred, the resulting plasma profile is inserted back into the radiation-hydrodynamics code; the simulation is then resumed, and the fusion performance of the (heated) implosion can thus be determined. Implementing this heating would require the generation of an electron beam with appropriate properties, and this has not yet been studied in

detail. The most promising way to produce such a beam would be to irradiate the compressed fuel assembly with a single ultra-intense short-pulse laser, but further study is required to investigate whether this would generate an electron distribution function with the required 'bump-on-tail' to drive the heating instability.

This auxiliary heating process has been demonstrated in Vlasov and PIC simulations in [18, 19], but has not yet been verified experimentally. However, it is worth noting that collisionless heating via counter-propagating electron beams was previously demonstrated in [29]. This heating was due to a different process than considered here; in that work, the counter-propagating electron currents led to magnetic filaments due to the Weibel instability, which led to enhanced trapping of sub-2 MeV electrons within the hotspot. This process was estimated to result in an impressive 14% of the laser energy being transferred to the hotspot, which suggests that efficient transfer of energy between short-pulse lasers and plasma via electron-beams is indeed possible. This mechanism is distinct from the the process described in [18, 19] (which did not observe filamentation in their simulations) and considered in this article, where the transfer of energy from beam to background plasma is due to the growth and damping of Langmuir waves. The key difference between these approaches is the electron distribution function used. The electron distribution function in the experimental work [29] (obtained from their simulations) is not capable of driving the 'bump-on-tail' instability and thus this heating process would not be expected to feature in their experiment, while [18, 19] feature profiles that are designed to generate such an effect (as stated previously, the generation of such an electron distribution from short-pulse laser interactions remains an area of active research). The conditions in the experimental work [29] are also significantly cooler and less dense than considered in [18, 19] (this lower density is significant, as a high density is required to give a high electron-ion collision rate and thus rapid temperature equilibration). Despite these differences the work presented in [29] is a significant and highly relevant result, due to it's demonstration of collisionless heating of an implosion and the high efficiency they achieved. Further research is recommended into both heating techniques, and it is noted that the Weibel instability could provide an alternative mechanism for depositing electron energy into the hotspot and therefore driving auxiliary heating.

This article aims to interpret the results of [16, 19, 26] analytically, to further increase understanding of these two approaches (low convergence implosions and auxiliary heating). In section 2, a standard hot-spot ignition model is shown to be applicable to describing fixed convergence ratio implosions, and is then applied to model the results of [26]. Meanwhile, section 3 demonstrates how a simple argument based on the burn-up of DT fuel can be used to understand auxiliary heating, and make qualitative predictions about how different implosions will respond to this technique. This is tested by applying auxiliary heating to a number of well-performing (i.e. high yield/gain) implosions, and the gain achieved when such heating is applied to these implosions in then discussed in section 4. Section 5 then summarizes and concludes the paper.

2. Gain scaling of fixed convergence ratio capsules

In [16], implosions were optimized for a number of different capsules within a 'low-instability' regime, defined by limits to convergence ratio, implosion velocity, in-flight aspect ratio (IFAR), and laser intensity. A range of capsule radii were considered, resulting in implosions with a range of required laser energies and achieved fusion gains. In this section, a simple analytic model is applied to describe the performance achieved in these implosions.

The model used here is the hot-spot ignition model for isobaric fuel configurations presented by Meyer-Ter-Vehn [30, 31], developed following previous efforts by Kidder and Bodner [32, 33]. While more recent analytic modeling efforts have significantly further developed understanding of ICF implosions (for example, [34–40]), this model remains a useful approximation that can be simply adapted for the purposes of this work. The full derivation is not repeated here, but the key details are briefly summarized. The fuel is compressed by a laser driver with energy E_d to a compressed fuel radius of R_f. The compressed fuel is modeled as two distinct regions: an inner hotspot region between $0 < R < R_\mathrm{h}$ with a uniform (low) density ρ_h and (high) temperature T_h, and a surrounding compressed shell between $R_\mathrm{h} < R < R_\mathrm{f}$ with a uniform (high) density ρ_c and (low) temperature T_c. This fuel assembly is isobaric, with a uniform pressure p across both hotspot and shell. It is assumed that ignition occurs, and thus that the hotspot temperature and areal density are described by the ignition conditions. In this paper, the conditions assumed in [31] are used:

$$T_\mathrm{h} = 8\,\mathrm{keV}, \tag{1}$$

$$H_\mathrm{h} = \rho_\mathrm{h} R_\mathrm{h} = 0.25\,\mathrm{g\,cm^{-2}}. \tag{2}$$

The model results in an equation for the gain G of

$$G = \frac{4\pi}{3}\frac{q_\mathrm{DT}}{E_\mathrm{d}}\left[\rho_\mathrm{h}R_\mathrm{h}^3 + \rho_\mathrm{c}\left(R_\mathrm{f}^3 - R_\mathrm{h}^3\right)\right]\frac{H_\mathrm{h}+H_\mathrm{c}}{H_\mathrm{b}+H_\mathrm{h}+H_\mathrm{c}}, \tag{3}$$

where

$$R_\mathrm{h} = \mathcal{F}_\mathrm{DT}/p, \tag{4}$$

$$R_\mathrm{f} = \left(\eta E_\mathrm{d}/2\pi p\right)^{1/3}, \tag{5}$$

$$\rho_\mathrm{h} = H_\mathrm{h} p/\mathcal{F}_\mathrm{DT}, \tag{6}$$

$$\rho_\mathrm{c} = \left(\alpha A_\mathrm{deg}\right)^{-3/5} p^{3/5}, \tag{7}$$

$$H_\mathrm{c} = \rho_\mathrm{c}\left(R_\mathrm{f} - R_\mathrm{h}\right), \tag{8}$$

$$\mathcal{F}_\mathrm{DT} = 2H_\mathrm{h}T_\mathrm{h}k_\mathrm{B}/\mu_{DT}, \tag{9}$$

$$H_\mathrm{b} = 8c_\mathrm{s}\mu_\mathrm{DT}/\langle\sigma\nu\rangle \approx 7\,\mathrm{g\,cm^{-2}}. \tag{10}$$

α is the adiabat of the implosion, while η is the hydrodyanmic efficiency (i.e. the fraction of laser energy converted into fuel energy at the time of ignition). $\mathcal{F}_\mathrm{DT}$ is a collection of terms, and is constant for a given set of hotspot conditions T_h and H_h. k_B is Boltzmann's constant, $\mu_\mathrm{DT} = 4\times10^{-24}$ g is the average atomic fuel mass, $q_\mathrm{DT} = 3.37\times10^{11}$ J g^{-1} is the fusion energy released per fuel mass burnt, and $A_\mathrm{deg} = 2.17\times10^{12}$ (erg/cm^{-3})/(g cm^{-3})$^{5/3}$ is the constant of proportionality used in calculating the adiabat from the ratio of actual

fuel pressure to degenerate pressure. H_b is the burn-up parameter used to approximate the burn-up fraction of DT fuel, where c_s is the sound speed and $\langle\sigma\nu\rangle$ is the DT reactivity. Both c_s and $\langle\sigma\nu\rangle$ (and thus also H_b) contain a temperature dependence, but for igniting implosions it is typically assumed that this can be ignored and a constant value of $H_b = 7\ \mathrm{g\ cm^{-2}}$ used instead.

Assuming values for T_h and H_h leaves only three free parameters when using equation (3) to estimate the relationship between gain and driver energy E_d: the fuel stagnation pressure p, the adiabat α, and the hydrodynamic efficiency η. The general application of this model is to specify these three parameters for a given implosion, and then to produce gain curves of G vs E_d. Such curves correspond to implosions of increasing energy but a constant fuel pressure, and (through equation (4)) to a constant hotspot radius. The hotspot and shell densities remain unchanged, but the overall radius of the compressed fuel increases (as it is related to the drive energy through equation (5)). This necessitates an increased capsule mass, which corresponds to an increase in initial capsule radius R_i). This increasing initial radius but constant hotspot radius means the convergence ratio $\mathrm{CR} = R_i/R_h$ must therefore also be increasing.

In order to adapt this model to produce curves describing implosions with fixed convergence ratio, one must consider how such implosions scale as the laser energy changes. The optimized implosions in [16] are observed to closely follow the hydrodynamic scaling relations [36], as discussed in [26]. These implosions are essentially scale versions of one another, where all radii within the capsule increase proportionally as the initial outer radius is scaled. As the convergence ratio is constant, the hotspot radius must also scale accordingly. This can be expressed simply as $R_h \propto R_i$. In addition to this, the hydrodynamic scaling relations identify the scaling between the drive energy of the capsule and the initial radius as $E_d \propto R_i^3$. Taking these two relationships together results in an additional equation to the set

$$R_h \propto E_d^{1/3}. \tag{11}$$

This new equation removes p as a free parameter; R_h is instead now determined based on E_d, and this determines the pressure accordingly through equation (4). A single simulation must be used first to give a pair of R_h and E_d values from which the constant of proportionality in equation (11) can be determined. This constant is then used to describe scaled versions of that implosion according to the hydrodynamic scaling relations, and thus equation (3) can be used to produce curves of gain for such implosions as a function of E_d (for fixed values of η and α).

Figure 1 displays the calculated gain scaling curve for the third-harmonic implosions from [16, 26], where the 8.4 MJ implosion from [16] was used to determine the constant of proportionality in equation (11). The adiabat α was calculated for these implosions according to the method described in [37], and found to vary between 2.5 and 3.5. For the curves in figure 1, an α of 2.8 and an assumed efficiency of 7% (a reasonable estimate for direct drive implosions [31]) were used;

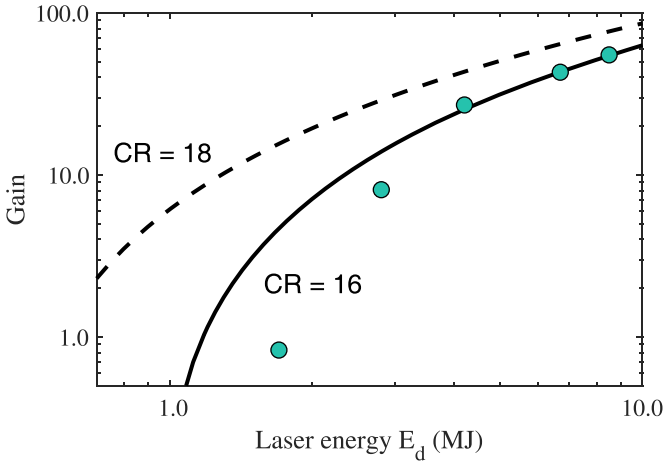

Figure 1. Gain curve for a fixed convergence ratio of 16 (solid curve) calculated using the analytic model, for an α of 2.8 and an η of 0.07. The teal points corresponds to the optimized implosions in this regime simulated in [16, 26]. The dashed curve represents the model for a convergence ratio of 18.

these were found to give a good fit to the highest energy implosions. However, the model is seen to significantly overestimate the performance of the lower energy implosions. This is because it assumes that ignition is occurring, and the value of many of the constants within it are set by ignition physics and assumes that the ion temperature is at least 8 keV. In particular, the use of a constant H_b assumes that the burn-up fraction for each implosion (in reality a function of temperature) is near to it is limiting value; this is shown not to be the case for the lower energy implosions in the subsequent section. However, as this model clearly does a good job of predicting the performance of the well-igniting implosions, it thus provides a useful upper limit on the performance of fixed convergence ratio implosions.

This model also allows the performance of implosions with different convergence ratios to be estimated without performing the type of extensive optimization campaign presented in [16]. The dashed curve in figure 1 shows the performance if the convergence ratio is instead increased to 18, while maintaining the same adiabat and efficiency (since the constant of proportionality in equation (11) relates the hotspot radius to the outer radius this constant must be inversely proportional to the convergence ratio, and thus the new curve was obtained by multiplying it by 16/18). It can be seen that doing so significantly increases the achievable gain of the implosions. However, it is worth bearing in mind that a) increasing the convergence ratio will likely result in less agreement between these predictions and experimental performance, and b) this change may also affect the IFAR and implosion velocities (which do not appear explicitly in these equations), which could again increase susceptibility to instability growth. This behavior is all described in the scaling between drive energy and hotspot radius given in equation (11), and so a more accurate gain curve ensuring the appropriate IFAR and implosion velocity could be obtained by optimizing a single implosion for a given convergence ratio to determine the appropriate constant of proportionality.

Table 1. Basic details of the implosions considered in this paper, full details of which are available in [16, 26]. Size multiplier is a linear scaling factor applied to the capsule radius (where a size multiplier of 1 corresponds to a radius of 2.85 mm). All measured quantities are given to two significant figures. Note that the gain for some capsules is slightly changed from previously published results, due to updates to HYADES since that work was performed.

Capsule label	A	B	C	D	E	F	G	H
Laser driver	——————Third-harmonic——————						Two-colour	ArF
Size multiplier	0.25	0.35	0.5	0.65	0.75	0.85	0.5	0.5
'Long-pulse' laser energy (MJ)	0.10	0.27	0.77	1.7	2.8	4.2	1.7	1.9
Gain	0.030	0.067	0.19	0.83	8.1	27	5.4	19
Burn-up percentage	0.012	0.029	0.099	0.35	3.6	16	4.7	19

3. Understanding auxiliary heating through the burn-up fraction

In [26], auxiliary heating was applied to a number of sub-ignition implosions, and in each case was shown to amplify the fusion yield. These implosions are briefly summarized in table 1, where they are given the same labels A-D as in [26] (implosions E-H are additional implosions not considered previously, and discussed later). For each implosion, the effect of auxiliary heating was simulated by adding electron energy to central zones within the implosion over a 7 ps time period. Simulations were performed where the time at which this injection began was varied, and an optimal time for each implosion was identified (this typically occurred just prior to stagnation). Then further simulations were performed for each implosion, varying the injected electron energy at this optimal time between 0 and 60 kJ. As expected, applying auxiliary heating led to an increase in the ion temperature in the hotspot, which in turn resulted in an increased number of fusion reactions. The aim of this approach was to push the implosions over the ignition threshold, and for implosion D (the highest energy implosion considered, with the largest capsule and the highest unheated gain) this was successful. This implosion achieved break-even when auxiliary heating was applied, and as the heating energy increased the gain improved substantially.

Figure 9 in [26] plotted the relative yield amplification against the deposited electron energy for the four different implosions A-D, of increasing capsule radius, laser energy, and fusion yield. The relative yield amplification was shown to be most substantial for the smallest implosions, which makes sense for two reasons: (1) the smallest capsules have the lowest yield, and so a smaller increase is required for a given relative increase; and (2) the smallest capsules have less mass, and thus the heating energy added per DT pair is higher. If instead the yield amplification is considered in terms of the deposited electron energy divided by the DT fuel mass (i.e. scaling to remove the influence of the larger capsule size), one finds that the yield amplification actually increases with the capsule size and implosion energy. In this section, this phenomenon is explored.

First, a simple (and commonly used) analytic framework for the fusion yield and burn-up of DT fuel is discussed, before being applied to auxiliary heating. The yield Y of an inertial fusion implosion can be simply expressed as

$$Y = \Phi\ M_{\mathrm{DT}}\ q_{\mathrm{DT}}\ , \tag{12}$$

where M_{DT} is the DT fuel mass and q_{DT} is the energy released in each DT fusion reaction. Φ is the burn-up fraction (often multiplied by 100 to give a burn-up percentage), or the fraction of DT pairs in the capsule that have undergone fusion. This quantity is commonly approximated using the formula

$$\Phi = \frac{\rho R}{\rho R + H_{\mathrm{b}}}\ , \tag{13}$$

where ρR is the integral of density over the capsule radius, and H_{b} is a collection of terms referred to as the 'burn-up' parameter described in (14). H_{b} has a strong temperature dependence, but (as in the previous section) this is often ignored and a constant value of $H_{\mathrm{b}} = 7\ \mathrm{g\,cm^{-2}}$ is used; this assumes that the implosion ignites and reaches a temperature of around 20 keV, and thus the burn-up is close to maximal. The expression for H_{b} used here is the one presented in [41], where

$$H_{\mathrm{b}} = 0.866\ \sqrt{T_{\mathrm{burn}}}\ \exp\left(0.572\ \ln\left(\frac{64.2}{T_{\mathrm{burn}}}\right)^{2.13}\right). \tag{14}$$

T_{burn} is the 'burn-averaged' ion temperature in keV, which can be calculated

$$T_{\mathrm{burn}}\ =\ \frac{\int\int T(R,t)\cdot e\,(R,t)\ \mathrm{d}^3R\ \mathrm{d}t}{\int\int e\,(R,t)\ \mathrm{d}^3R\ \mathrm{d}t}\ , \tag{15}$$

where t represents time. $e(R,t)$ is the burn rate per unit volume, and thus the denominator of equation (15) is the total yield [41]. The spatial and temporal integration means that T_{burn} is an unambiguous single value for a given implosion, which can be easily calculated from simulations (and is the reason that this formulation of H_{b} is used in place of alternative equations, such as that in [42]). It is important to note that the burn-up formula (equation (13)) is approximate, and its derivation (presented in [43, 44]) includes a number of assumptions; these include assuming the hotspot to be at a single uniform temperature, and approximating the burn wave as propagating at a few times the sound speed. This model also

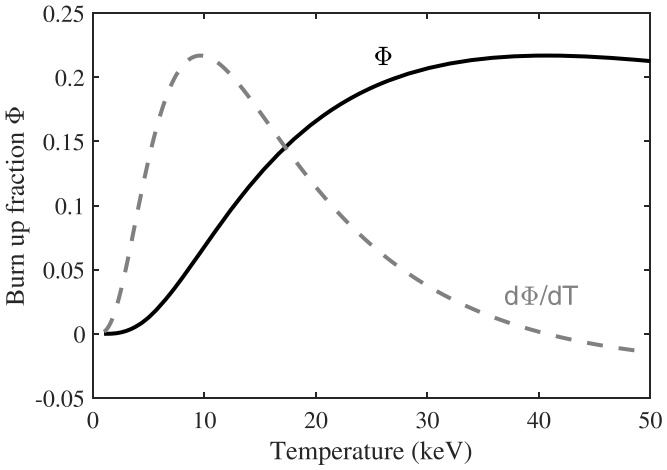

Figure 2. Burn-up fraction for an areal density of 1.7 g cm^{-2}. The grey dashed line shows the gradient of this curve with respect to temperature (not to scale). Changing the areal density changes the magnitude of these curves, but the general shape does not change significantly.

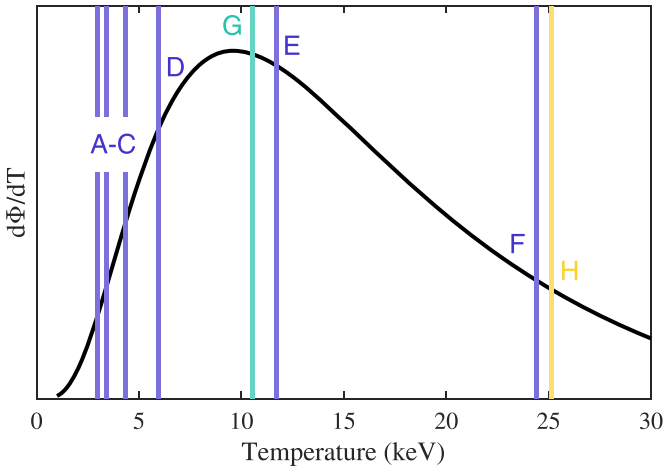

Figure 3. Gradient of the theoretical burn-up fraction vs temperature, with vertical markers signifying the temperature achieved in the different implosions. Dark blue lines (A–E, F) indicate third-harmonic implosions, while the teal line (G) indicates a two-color implosion and the yellow line (H) indicates an ArF implosion. Those implosions corresponding to higher dΦ /dT values are expected to show the most improvement when auxiliary heating is applied.

assumes a freely expanding DT sphere; in reality the expansion is tamped, and thus the burn fraction can be higher than the model predicts [30].

The impact of auxiliary heating on a given implosion can be considered through these equations. M_{DT} is set by the capsule and therefore does not change with the application of auxiliary heating, and thus the effect of this technique is described fully by its impact on the burn-up fraction. However, as auxiliary heating is applied late in the implosion once the hotspot and shell have been assembled, the areal density is also assumed to be unaffected. The change in burn-up fraction is thus due solely to the increased temperature. A plot of the burn-up percentage as a function of temperature is shown in figure 2 for a capsule with an areal density of 1.7 g cm^{-2}, and demonstrates how the burn-up changes with this parameter. While changing the areal density has a significant effect on the magnitude of this curve, the general shape is relatively consistent.

Unfortunately, it is not simple to predict quantitatively the increase in temperature and thus burn-up that a given amount of deposited energy will have. This problem is non-linear due to the nature of ignition. In addition, the burn-up fraction equation is approximate and does not give the burn-up to high accuracy. However, it can be used qualitatively to predict where auxiliary heating is likely to be most effective. If the unheated implosion has a burn-averaged temperature where the burn-up fraction is changing rapidly, then a small increase in temperature will have a more substantial impact on the burn-up fraction than otherwise. In other words, auxiliary heating will be most effective in regions where the gradient dΦ /dT is high. dΦ /dT is indicated by the dashed curve in figure 2.

This suggests that the effectiveness of auxiliary heating can potentially be qualitatively predicted based on the burn-averaged temperature of the unheated implosion, and the relative value of dΦ /dT at that temperature. While the value of dΦ /dT will vary based on the areal density, the general shape of the curve and the position of the peak do not change significantly, and thus general trends can be identified. To explore this further, the implosions A-H in table 1 are considered. This includes the third-harmonic implosions A-D to which heating was applied in [26], along with two additional third-harmonic implosions implosions E and F, the 'two-color' implosion G, and the ArF driven implosion H. These four additional implosions were also presented in [26], but without auxiliary heating; the ArF driven implosion used a 193 nm laser driver with the same four-pulse sequence, while the 'two-color' implosion featured an initial four-pulse third-harmonic drive, supplemented with a single higher intensity pulse at the ArF frequency late in the implosion (this captured some of the benefits of the high frequency driver, while relying on the more mature third-harmonic laser for the majority of the drive energy). These implosions all occupy the low-instability regime, although the use of higher frequency drivers permits higher peak intensities to be used. These four newly considered implosions have gains significantly higher than 1, allowing the performance for igniting capsules to be considered. The use of different laser drivers in these simulations means that implosions C, G and H feature capsules with the same outer radius (and thus similar laser energies), while having substantially different burn-up fractions and gains.

Figure 3 again shows a plot of dΦ /dT (specifically for an areal density of 1.7 g cm^{-2}, but the areal density is not too significant when considering only the shape of the curve), but with the burn-averaged temperature for the implosions A–H indicated. It can be seen that moving from implosion A to D sees the value of dΦ /dT increase, which explains the increase in effectiveness of the heating across these four implosions discussed at the start of the section. As T increases further, dΦ /dT is seen to peak at around 10 keV. Implosions E and G have burn-averaged temperatures very close to this value, suggesting that these implosions will likely experience the maximum

benefit from auxiliary heating. The value of $d\Phi/dT$ begins to decrease past 10 keV, although it remains high over a wide temperature range. This suggests that auxiliary heating will be less effective for F than for E and G, and will have the least impact on implosion H.

The predictive capability of this approach was tested by simulating the effect of auxiliary heating in radiation hydrodynamic simulations (using the code HYADES [45]) of implosions E-H, following the process described in [26]. The resulting burn-up percentage (calculated exactly using the simulation results, rather than estimated using the analytic burn-up formula) of the heated implosions as a function of the deposited electron energy per unit mass is displayed in figure 4. These results match well with the predictions based on the previous analysis. Implosions E and G both respond very well to the heating, and show a similar substantial improvement in burn-up fraction. This is a greater increase than was experienced by implosion D. Implosion D in turn outperforms implosion C, as well as implosions A and B (these are omitted from the plot, but fit the observed trend). As expected, implosion F shows a smaller increase than E and G (although still substantial), while implosion H does not increase significantly. It is worth reiterating here that implosions G and H are substantially different than A-D due to the different laser drivers, with implosion F having a higher yield and gain than implosion H (a gain of 24 compared to 19). The fact that F responds better to the heating than H despite this clearly demonstrates that it is the burn-up fraction that is important in predicting response to auxiliary heating, rather than the gain or yield. Figure 4 shows that it is indeed possible to explain the effectiveness of auxiliary heating through the burn-up fraction and burn-averaged temperature, and that this can be qualitatively predicted through analysis of the relative magnitude of $d\Phi/dT$ for the particular burn-averaged temperature of the unheated capsule. In addition, it appears that auxiliary heating results in significant improvements to burn-up fraction for a wide range of implosions, corresponding to burn-averaged temperatures in the roughly 5–20 keV range.

The saturation behaviour in figure 4 is also interesting. For the low burn-up implosions, the increase in burn-up percentage with increased electron energy is reasonably linear (and the gradient can even increase for larger amounts of injected energy), while for the larger burn-up capsules a saturation in burn-up is observed. This makes intuitive sense through the burn-up model; for the low burn-up capsules $d\Phi/dT$ is increasing with temperature, which means that auxiliary heating becomes more effective as more energy is added. For those implosions past the peak of $d\Phi/dT$, the change in $d\Phi/dT$ with temperature is negative and thus auxiliary heating becomes less effective as more is added. However, this model does not fully explain this behaviour. Consider implosion E, which has clearly started to become asymptotic for the highest amounts of heating. When 60 kJ of electron energy has been injected the burn-averaged temperature of E is 20 keV, and so it makes sense that further heating beyond this is less effective in increasing the burn-up percentage. However, implosion F has a higher burn-averaged temperature of 24 keV without any heating, yet still sees a reasonable increase in burn-up percentage when heating is first applied. This demonstrates that such saturation behavior cannot be fully explained through this model alone. This is likely because the burn-up model is approximate and does not estimate the burn-up fraction to high accuracy, with effects such as tamping of the fuel meaning that real implosions will feature different burn-up fractions than predicted [30]. As evidence of this, the simulated burn-up fraction for implosion F (without heating) is 19%, while the burn-up model predicts a peak possible burn-up of only 15.2%. While this model is therefore clearly useful in estimating the rough values of burn-up fraction and can be used to suggest where auxiliary heating is most useful, it must be remembered that the trends in $d\Phi/dT$ are approximate only, and therefore cannot be used to fully describe the complete burn-up behaviour.

Finally, it is worth noting again that whether an implosion will respond well to the heating is ascertained through $d\Phi/dT$, and this increase is measured through the change in Φ, but Φ is not used to determine the effectiveness directly. This is because the value of the burn-up fraction will change dramatically with the areal density of the capsule, and thus it is unclear from Φ alone whether the capsule has a low areal density but high temperature (and so will not respond well to auxiliary heating), or a high areal density and a low temperature (and thus will respond well). Figures such as figure 4 must therefore be interpreted with caution, as implosions may have a similar burn-up fraction to begin with, but have a very different response when auxiliary heating is applied.

4. Estimated gain for the new heated implosions

The discussion so far has related to the general effectiveness of auxiliary heating. The impact that this heating has on the gain of these implosions—the overall metric of interest for IFE—will now be considered.

The difficulties of estimating the gain for auxiliary heating simulations in hydrodynamics codes (where the heating is treated simply as deposited electron energy) were discussed in [26]. In short, one must estimate the efficiency with which electron beams can be generated and transported to the hotspot, and the efficiency with which energy from this beam is donated to the plasma. The necessary short-pulse laser energy to produce the electron energy deposited in the simulation can thus be approximated, and added to the 'long-pulse' laser energy in the simulation to estimate the total laser energy. This is in turn used to estimate the gain.

Figure 5 displays this estimated gain against total laser energy for implosions C-F, assuming as in [26] an overall efficiency of 9.6% (an efficiency of 52% from [46] for production and transport of the beams, and an efficiency of 18% from [18, 19] for coupling between the beams and hotspot). Figure 5 further highlights many of the trends seen in figure 4, as the trend in yield follows that of burn-up fraction, but the energy cost of the heating is now included. It is seen that regions of figure 4 where the burn-up percentage increased rapidly with deposited electron energy see significant increases in gain when the heating is applied, while regions where the increase is small

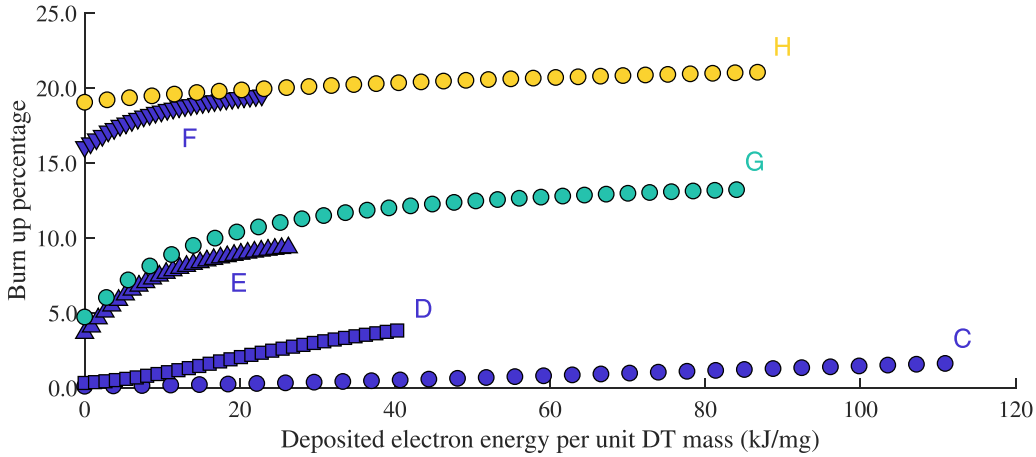

Figure 4. Burn-up percentage achieved in the simulations for a range of implosions, as a function of the deposited electron energy per DT unit mass. Blue curves (C)–(F) represent third-harmonic implosions, teal curves (G) two-colour implosions, and yellow curves (H) ArF implosions. Shapes indicate capsule size, with circles (C), (G), (H) representing 0.5 scale capsules, squares (D) 0.65, upwards pointing triangles (E) 0.75, and downward pointing triangles (F) 0.85. For each implosion, the first point represents the simulation without heating, and the last point includes 60 kJ of deposited electron energy.

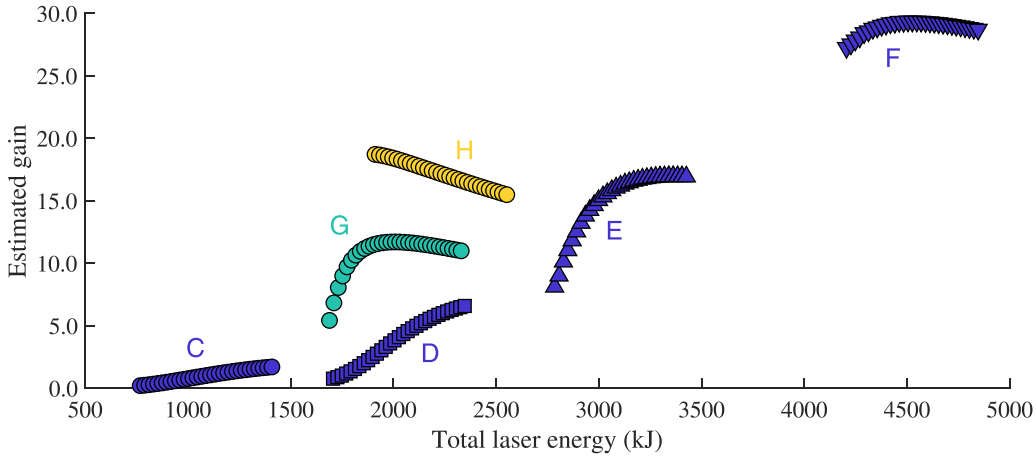

Figure 5. Estimated gain as a function of total laser energy. It is assumed that short-pulse laser interactions are used to generate electron beams that deposit the electron energy added in the simulation, with an overall efficiency for this process of 9.6%, as explained in [26]. This short pulse laser energy, plus the 'long-pulse' laser energy featured in the simulation and listed in table 1, is then used to calculate the gain of each implosion. Colors and shapes are again used to represent laser driver and capsule size, as explained in figure 4. For each implosion, the first point represents the simulation without heating, and the last point includes 60 kJ of deposited electron energy.

or negligible thus see the gain decrease (as the increase is outweighed by the additional energy cost). In addition, the most significant increases are seen for implosions E and G (where gain increases from 8.1 to 17, and from 5.4 to 12, respectively), as expected based on the previous analysis. It also highlights that whether auxiliary heating will improve performance is not a function of gain, with implosion F demonstrating a greater increase in gain when heating is applied than implosion H. Most significantly, it demonstrates that auxiliary heating can be a useful technique for improving gain beyond sub-ignition capsules, with implosions E and G in particular demonstrating significant increases despite their high gain prior to heating. Substantial increases are observed for these capsules for relatively small amounts of heating; for 20 kJ of deposited electron energy (or ∼210 kJ of short pulse laser energy under the current assumptions), implosion E reaches a gain of 15, and G a gain of 11. This demonstrates that even as implosions begin to achieve ignition (as recently demonstrated on the NIF), auxiliary heating could continue to be a useful technique to improve performance.

5. Conclusions

The research presented in this article significantly aids the understanding and interpretation of previous results regarding low convergence ratio implosions and auxiliary heating. In section 2, it was shown that standard hot-spot ignition models can be used to derive gain scaling relations for fixed convergence ratio implosions, such as those presented in [16]. This significantly reduces the number of simulations required to estimate curves of gain vs laser energy for capsules of a given

convergence ratio, as only one data point is required to obtain the constant of proportionality (many thousands of simulations were performed in [16] to optimise the data points plotted in figure 1). Then, in section 3, it was shown how the effect of auxiliary heating on an implosion can be understood simply through the change that the corresponding increase in burn-averaged temperature has on the burn-up fraction of an implosion. It was shown that the derivative of burn-up fraction with respect to temperature can be used to qualitatively predict how effective auxiliary heating is likely to be, with the best results for implosions with burn-up temperatures in the 5–20 keV range. This was then tested by applying auxiliary heating to a range of new implosions beyond those considered in previous work, and it was found that this approach was indeed successful in qualitatively predicting performance.

The gain of the new implosions, when heated using this technique, were then estimated assuming a 9.6% overall heating efficiency. It was found that the heating performance agreed well with the qualitative predictions from the previous analysis. Auxiliary heating was shown to be able to substantially improve the gain for already well-performing implosions, depending on the burn-up temperature of the implosion. Particular benefit was observed for implosions E and G, where gain increased from 8.1 to 17, and from 5.4 to 12, respectively-with most of this increase occurring for only 20 kJ of deposited electron energy. This not only demonstrates the validity of interpreting auxiliary heating through the burn-up model and the ability to use this approach to identify implosions well-suited to auxiliary heating, but also highlights that this technique is not limited to sub-ignition capsules, and thus remains relevant to IFE efforts even in light of recent ignition results.

Data availability statement

All data that support the findings of this study are included within the article (and any supplementary files).

Acknowledgments

The authors gratefully acknowledge the support of the staff of the Central Laser Facility and Scientific Computing Department, UKRI-STFC Rutherford Appleton Laboratory and the Orion laser facility at AWE plc in support of this work. They would also like to thank R S Craxton for his detailed comments on the manuscript, along with with T J B Collins, V N Goncharov, J T Larsen and R Manson-Sawko for a number of useful discussions. This work was supported by the 0014023 STFC IAA Starter/Accelerator Fund grant and the John Adams Institute Grant ST/V001655/1.

ORCID iDs

R W Paddock https://orcid.org/0000-0002-0712-9283
R T Ruskov https://orcid.org/0000-0001-9205-2585
S Hughes https://orcid.org/0000-0001-9985-3908
C D Murphy https://orcid.org/0000-0003-3849-3229
R Bingham https://orcid.org/0000-0002-9843-7635
A B Zylstra https://orcid.org/0000-0003-0489-7479
T Goffrey https://orcid.org/0000-0003-0784-1294
T D Arber https://orcid.org/0000-0002-9322-4913
P A Norreys https://orcid.org/0000-0002-5539-9464

References

[1] Abu-Shawareb H *et al* 2022 Criterion for ignition exceeded in an inertial fusion experiment *Phys. Rev. Lett.* **129** 075001
[2] Kritcher A L *et al* 2022 Design of an inertial fusion experiment exceeding the Lawson criterion for ignition *Phys. Rev.* E **106** 025201
[3] Zylstra A B *et al* 2022 Experimental achievement and signatures of ignition at the National Ignition Facility *Phys. Rev.* E **106** 025202
[4] Zylstra A B *et al* 2022 Burning plasma achieved in inertial fusion *Nature* **601** 542–8
[5] Bishop B 2022 Lawrence Livermore National Laboratory achieves fusion ignition (available at: www.llnl.gov/archive/news/lawrence-livermore-national-laboratory-achieves-fusion-ignition)
[6] Campbell E M *et al* 2017 Laser-direct-drive program: promise, challenge and path forward *Matter Radiat. Extremes* **2** 37–54
[7] Goncharov V N, Igumenshchev I V, Harding D R, Morse S F, Hu S X, Radha P B, Froula D H, Regan S P, Sangster T C and Campbell E M 2020 Novel hot-spot ignition designs for inertial confinement fusion with liquid-deuterium-tritium spheres *Phys. Rev. Lett.* **125** 065001
[8] Tynan G R and Abdulla A 2020 How might controlled fusion fit into the emerging low-carbon energy system of the mid-twenty-first century? *Phil. Trans. R. Soc.* A **378** 20200009
[9] Gi K, Sano F, Akimoto K, Hiwatari R and Tobita K 2020 Potential contribution of fusion power generation to low-carbon development under the Paris Agreement and associated uncertainties *Energy Strategy Rev.* **27** 100432
[10] Akli K *et al* 2023 Report of the fusion energy sciences workshop on inertial fusion energy *Technical Report* US Department of Energy Office Of Science
[11] Olson R E *et al* 2021 A polar direct drive liquid deuterium-tritium wetted foam target concept for inertial confinement fusion *Phys. Plasmas* **28** 122704
[12] Olson R E *et al* 2016 First liquid layer inertial confinement fusion implosions at the National Ignition Facility *Phys. Rev. Lett.* **117** 245001
[13] Igumenshchev I V *et al* 2023 Proof-of-principle experiment on the dynamic shell formation for inertial confinement fusion *Phys. Rev. Lett.* **131** 015102
[14] Haines B M *et al* 2017 The effects of convergence ratio on the implosion behavior of DT layered inertial confinement fusion capsules *Phys. Plasmas* **24** 072709
[15] Zylstra A B *et al* 2018 Variable convergence liquid layer implosions on the National Ignition Facility *Phys. Plasmas* **25** 056304
[16] Paddock R W *et al* 2021 One-dimensional hydrodynamic simulations of low convergence ratio direct-drive inertial confinement fusion implosions *Phil. Trans. R. Soc.* A **379** 20200224
[17] Norreys P A 2014 Auxiliary heating of inertial confinement fusion targets *Bull. Am. Phys. Soc.* **59** 15
[18] Ratan N, Sircombe N J, Ceurvorst L, Sadler J, Kasim M F, Holloway J, Levy M C, Trines R, Bingham R and Norreys P 2017 A Dense plasma heating by crossing relativistic electron beams *Phys. Rev.* E **95** 013211

[19] Lee J J *et al* 2023 Toward more robust ignition of inertial fusion targets *Phys. Plasmas* **30** 022702
[20] Lampe M and Sprangle P 1975 Saturation of the relativistic two-stream instability by electron trapping *Phys. Fluids* **18** 475–81
[21] Drummond W E, Malmberg J H, O'Neil T M and Thompson J R 1970 Nonlinear development of the beam-plasma instability *Phys. Fluids* **13** 2422–5
[22] Thode L E and Sudan R N 1975 Plasma heating by relativistic electron beams. I. Two-stream instability *Phys. Fluids* **18** 1552–63
[23] Mendonça J T, Norreys P, Bingham R and Davies J R 2005 Beam instabilities in laser-plasma interaction: relevance to preferential ion heating *Phys. Rev. Lett.* **94** 245002
[24] Everett M J, Lal A, Clayton C E, Mori W B, Joshi C and Johnston T W 1996 Coupling between electron plasma waves in laser-plasma interactions *Phys. Plasmas* **3** 2041–6
[25] Papadopoulos K 1975 Nonlinear stabilization of beam plasma interactions by parametric effects *Phys. Fluids* **18** 1769
[26] Paddock R W *et al* 2022 Pathways towards break even for low convergence ratio direct-drive inertial confinement fusion *J. Plasma Phys.* **88** 905880314
[27] Norreys P A, Ridgers C, Lancaster K, Koepke M and Tynan G 2021 Prospects for high gain inertial fusion energy: an introduction to the 2nd edn *Phil. Trans. R. Soc.* A **379** 20200028
[28] Lee J, Elisseev V, Manson-Sawko R, Paddock R W, Goffrey T, Arber T, Morris S, de Witt S and Norreys P A 2023 Multi-scale simulations of hot electron transport in overdense plasma *Sci. Rep.* submitted
[29] Mori Y *et al* 2016 Fast heating of imploded core with counterbeam configuration *Phys. Rev. Lett.* **117** 055001
[30] Meyer T V J 1982 On energy gain of fusion targets: the model of kidder and bodner improved *Nucl. Fusion* **22** 561
[31] Atzeni S and Meyer-ter Vehn J 2008 *The Physics of Inertial Fusion* (Oxford University Press)
[32] Kidder R E 1976 Energy gain of laser-compressed pellets: a simple model calculation *Nucl. Fusion* **16** 405
[33] Bodner S E 1981 Critical elements of high gain laser fusion *J. Fusion Energy* **1** 221
[34] Zhou C D and Betti R 2007 Hydrodynamic relations for direct-drive fast-ignition and conventional inertial confinement fusion implosions *Phys. Plasmas* **14** 072703
[35] Betti R, Chang P Y, Spears B K, Anderson K S, Edwards J, Fatenejad M, Lindl J D, McCrory R L, Nora R and Shvarts D 2010 Thermonuclear ignition in inertial confinement fusion and comparison with magnetic confinement *Phys. Plasmas* **17** 058102
[36] Nora R *et al* 2014 Theory of hydro-equivalent ignition for inertial fusion and its applications to OMEGA and the National Ignition Facility *Phys. Plasmas* **21** 056316
[37] Goncharov V N *et al* 2014 Improving the hot-spot pressure and demonstrating ignition hydrodynamic equivalence in cryogenic deuterium-tritium implosions on OMEGA *Phys. Plasmas* **21** 056315
[38] Betti R, Christopherson A R, Spears B K, Nora R, Bose A, Howard J, Woo K M, Edwards M J and Sanz J 2015 Alpha heating and burning plasmas in inertial confinement fusion *Phys. Rev. Lett.* **114** 255003
[39] Christopherson A R, Betti R, Bose A, Howard J, Woo K M, Campbell E M, Sanz J and Spears B K 2018 A comprehensive alpha-heating model for inertial confinement fusion *Phys. Plasmas* **25** 012703
[40] Christopherson A R, Betti R, Miller S, Gopalaswamy V, Mannion O M and Cao D 2020 Theory of ignition and burn propagation in inertial fusion implosions *Phys. Plasmas* **27** 052708
[41] Lindl J D, Haan S W, Landen O L, Christopherson A R and Betti R 2018 Progress toward a self-consistent set of 1D ignition capsule metrics in ICF *Phys. Plasmas* **25** 122704
[42] Bosch H S and Hale G M 1992 Improved formulas for fusion cross-sections and thermal reactivities *Nucl. Fusion* **32** 611–31
[43] Atzeni S, Schiavi A and Bellei C 2007 Targets for direct-drive fast ignition at total laser energy of 200-400 kJ *Phys. Plasmas* **14** 052702
[44] Fraley G S, Linnebur E J Mason R J and Morse R L 1974 Thermonuclear burn characteristics of compressed deuterium-tritium microspheres *Phys. Fluids* **17** 474–89
[45] Larsen J T and Lane S M 1994 HYADES-A plasma hydrodynamics code for dense plasma studies *J. Quant. Spectrosc. Radiat. Transfer* **51** 179–86
[46] Strozzi D J, Tabak M, Larson D J, Divol L, Kemp A J, Bellei C, Marinak M M and Key M H 2012 Fast-ignition transport studies: Realistic electron source, integrated particle-in-cell and hydrodynamic modeling, imposed magnetic fields *Phys. Plasmas* **19** 072711